Formation of a Tyrosyl Radical Intermediate in *Proteus mirabilis* Catalase by Directed Mutagenesis and Consequences for Nucleotide Reactivity†

Pierre Andreoletti,‡ Serge Gambarelli,§ Germaine Sainz,|| Vivian Stojanoff,|| Christopher White,‡,§ Gérard Desfonds,§ Jean Gagnon,§ Jacques Gaillard,§ and Hélène Marie Jouve*,‡

Institut de Biologie Structurale Jean-Pierre Ebel, CEA/CNRS/UJF, UMR 5075, 41 rue Jules Horowitz, 38027 Grenoble Cedex 1, France, Département de Recherche Fondamentale sur la Matière Condensée, SCIB-UMR 5046, CEA Grenoble, 17 rue des Martyrs, F-38054 Grenoble Cedex 9, France, and European Synchrotron Radiation Facility, 6 rue Jules Horowitz, BP 220, F-38043 Grenoble Cedex, France

Received April 4, 2001; Revised Manuscript Received September 18, 2001

ABSTRACT: *Proteus mirabilis* catalase (PMC) belongs to the family of NADPH binding catalases. The function of NADPH in these enzymes is still a matter of debate. This study presents the effects of two independent phenylalanine mutations (F194 and F215), located between NADPH and heme in the PMC structure. The phenylalanines were replaced with tyrosines which we predicted could carry radicals in a NADPH−heme electron transfer. The X-ray crystal structures of the two mutants indicated that neither the binding site of NADPH nor the immediate environment of the residues was affected by the mutations. Measurements using H_2O_2 as a substrate confirmed that the variants were as active as the native enzyme. With equivalent amounts of peroxoacetic acid, wild-type PMC, F215Y PMC, and beef liver catalase (BLC) formed a stable compound I, while the F194Y PMC variant produced a compound I which was rapidly transformed into compound II and a tyrosyl radical. EPR studies showed that this radical, generated by the oxidation of Y194, was not related to the previously observed radical in BLC, located on Y369. In the presence of excess NADPH, compound I was reduced to a resting enzyme ($k_{obs} = 1.7$ min^{-1}) in a two-electron process. This was independent of the enzyme's origin and did not require any thus far identified tyrosyl radicals. Conversely, the presence of a tyrosyl radical in F194Y PMC greatly enhanced the oxidation of reduced β-nicotinamide mononucleotide under a steady-state H_2O_2 flow with observable compound II. This process could involve a one-electron reduction of compound I via Y194.

Recently, considerable attention has been focused on the generation of protein radicals and their involvement in physiological or pathological processes. Several types of amino acid residues such as glycyl, cysteyl, tyrosyl, and tryptophanyl residues have been shown to form relatively stable radicals in proteins (*1*). These free radicals, involved in a variety of chemical reactions (*2*−*4*), can also have deleterious effects (*5*). In hydroperoxidases, the heme ferric iron reacts with a molecule of hydroperoxide to give compound I, containing an oxoferryl Fe(IV) group associated with a porphyrin π-cation radical. This compound is especially reactive in generating protein-based radicals (*6*−*9*). In catalases, compound I can be reduced either by two-electron donors such as hydrogen peroxide or by one-electron donors to give rise to compound II, an Fe(IV)−oxo (ferryl) species with saturated π-orbitals (*10*, *11*). Compound II is considered an inactive species in the H_2O_2 disproportion reaction. NADPH-dependent catalases use tightly bound NADPH[1] to protect themselves against inactivation as compound II species (*12*−*14*). However, whether it is compound I or compound II that reacts with the cofactor has not yet been established. A tyrosyl radical, observed in bovine liver catalase (BLC) and generated by the spontaneous decay of compound I, is suspected to be an intermediate (*12*, *15*−*17*). Calculations for electron tunneling pathways between NADPH and the heme iron by molecular dynamics using the X-ray crystal structure of BLC have shown that one of the most probable pathways involved amino acid residue Y214, near the NADPH binding site (*18*).

The catalase from *Proteus mirabilis* (PMC) is a NADPH-dependent catalase like BLC and human erythrocyte catalase (*19*, *20*) but can be easily prepared without bound NADPH, in contrast to the mammalian enzymes. Compound I of PMC is very stable, a property which has previously been used to

† This work was supported by the Commissariat à l'Energie Atomique (CEA) and by the Centre National de la Recherche Scientifique (CNRS).

* To whom correspondence should be addressed: Institut de Biologie Structurale Jean-Pierre Ebel, CEA/CNRS, VMR 5075, 41 Jules rue Horowitz, 38027 Grenoble Cedex 1, France. Phone: 33 (0) 438 78 95 78. Fax: 33 (0) 438 78 54 94. E-mail: jouve@ibs.fr.

‡ CEA/CNRS/UJF.

§ CEA Grenoble.

|| European Synchrotron Radiation Facility.

[1] Abbreviations: PMC, *P. mirabilis* catalase; PR, peroxide resistant; IPTG, isopropyl 1-thio-β-D-galactopyranoside; wt PMC, wild-type nonrecombinant PMC; BLC, bovine liver catalase; peracetic acid, peroxoacetic acid; Tris-HCl, tris(hydroxymethyl)aminomethane hydrochloride; NADH, β-nicotinamide adenine dinucleotide, reduced form; NADPH, β-nicotinamide adenine dinucleotide phosphate, reduced form; $NADP^+$, β-nicotinamide adenine dinucleotide phosphate, oxidized form; βNMNH, β-nicotinamide mononucleotide, reduced form; HRP, horseradish peroxidase; PDB, Protein Data Bank; rms, root-mean-square; Rz, A_{406}/A_{280} (nanometers), Reinheitszahl index; SDS−PAGE, sodium dodecyl sulfate−polyacrylamide gel electrophoresis; EPR, electronic paramagnetic resonance.

10.1021/bi010687f CCC: $20.00
Published on Web 10/18/2001

determine a high-resolution crystallographic structure of the enzyme in this particular state (*21*). It does not generate a tyrosyl radical intermediate. To clarify the reaction of catalase with NADPH and the hypothetical role of radicals in this reaction, two PMC variants with single mutations of phenylalanine to tyrosine (F194Y or F215Y) were made to reproduce the situation observed in BLC. The two phenylalanines were located between heme and NADPH (*22*). We present the high-resolution crystallographic structures of the two variants and their characterizations by UV−visible spectrophotometry and EPR spectroscopy. Reactivity studies with peracetic acid and under a steady-state flow of H_2O_2 are described, and the roles of different cofactors are identified. The results, compared with those already known for BLC and wild-type (wt) PMC, are discussed in relation to the mechanism of the reaction of catalase with NADPH and other nucleotides.

EXPERIMENTAL PROCEDURES

Chemicals. Catalase from from bovine liver (BLC) in crystalline suspension, lyophilized glucose oxidase from *Aspergillus niger*, β-nicotinamide adenine dinucleotide, reduced form (NADH), grade I, disodium salt, β-nicotinamide adenine dinucleotide phosphate, reduced form (NADPH), 98%, tetrasodium salt, and isopropyl β-D-thiogalactoside (IPTG) were purchased from Roche. β-Nicotinamide adenine mononucleotide, reduced form (βNMNH), 90%, sodium salt, and peracetic acid, 39% solution in acetic acid, were from Sigma-Aldrich. Hydrogen peroxide, 30% suprapur perhydrol, was from Merck. All chemicals were reagent grade.

Construction, Expression, and Purification of the F194Y and F215Y Mutants of PMC. F194Y and F215Y mutants of PMC were prepared by using the pALTER-Cat expression vector, as a template. The vector contained the catalase gene of *P. mirabilis* (*katA*) in the pALTER-*Ex*1 vector from Promega (*23*). Site-directed mutagenesis was performed by using the QuikChange kit from Stratagene. This method allows direct mutagenesis of the expression vector without subcloning in an intermediate vector. The pairs of complementary oligonucleotides (synthesized by Oligoexpress) were designed to introduce the required mutation (F to Y) and diagnostic restriction sites with silent mutations. The sens oligonucleotide of each pair was 5′-^{596}GCTATCGCTTTGTGCATGGT**TAT**GG*ATCC*CACACTTATAGC^{636}-3′ for the F194Y mutant and 5′-^{658}CGTTTCTGGGTTAAATTCCAT**TAT**CG*AT*GCCAACAAGGC^{696}-3′ for the F215Y mutant (mutated codons are in bold, silent mutations are in italic, and diagnostic restriction sites, *Bam*HI for F194Y and *Cla*I for F215Y, are underlined). Mutagnenesis was performed according to the manufacturer's protocol, and the reaction products were transformed into the *Escherichia coli* JM109 DE3 strain. Plasmids were purified with the mini-prep plasmid kit from Qiagen and digested with the diagnostic restriction enzymes to select positive clones. Sequencing of the complete catalase gene, carried out on plasmids of selected clones pAlter-Cat-F194Y and pAlter-Cat-F215Y, confirms that only the desired mutations occurred. Overexpression of recombinant wild-type and mutant catalases was achieved by growing the bacteria in Luria-Bertoni nutritive medium (LB) at 37 °C until the absorbance at 600 nm equaled 0.6. The catalase biosynthesis was induced by addition of 0.5 mM IPTG for 2 h with a reduced rate of shaking (130 rpm) to decrease the level of oxygenation of cultures and to slow the growth rates. Catalases were purified from *E. coli* using a method based on that previously described for the catalase of the peroxide resistant (PR) mutant of *P. mirabilis* (*20*). Only the forms without bound NADPH were used in this study, after having been carefully separated from those with NADPH. The obtained catalase preparations, the Rz index (A_{406}/A_{280}) of which was greater than 1.0, were highly purified as observed on SDS−PAGE. Protein solutions were concentrated to ≥50 mg/mL. Samples were stored at −20 °C after addition of glycerol to 8% (W/V).

Determination of Catalase Concentrations, Heme Content, and Catalytic Activity. Wild-type PMC was purified from *P. mirabilis* PR as described by Jouve et al. (*20*), and BLC was prepared according to the method of Ivancich et al. (*17*). The tetrameric concentrations of catalases were estimated spectrophotometrically using the following extinction coefficients: $\epsilon_{406} = 2.98 \times 10^5$ M^{-1} cm^{-1} for wt PMC (*24*) and $\epsilon_{405} = 3.24 \times 10^5$ M^{-1} cm^{-1} for BLC (*25*). Tetrameric catalase concentrations in mutated PMC were estimated using the ϵ_{280} (2.62×10^5 M^{-1} cm^{-1}) determined for wt PMC. Catalytic activities were measured spectrophotometrically by the decrease in absorbance at 240 nm of H_2O_2 at an initial concentration of 11 mM and expressed as the number of millimoles of H_2O_2 consumed per minute at 25 °C as previously described (*26*). Heme content was determined by the pyridine hemochromogen method (*27*), using the difference in absorbance between 556 and 580 nm measured on the redox difference spectrum where $\Delta(\Delta\epsilon^{red/ox})_{556-580} = 29$ mM^{-1} cm^{-1}.

Kinetic Measurements. The formation and decomposition of compounds I and II were followed by UV−visible spectrophotometry after the reaction of catalases (∼2 μM heme) with 1.5 equiv of peracetic acid in 0.1 M Tris-HCl buffer at pH 7.5 and 22 °C. The kinetics were determined from spectra recorded from 250 to 800 nm at regular time intervals on a Beckman DU 640 UV−visible spectrophotometer equipped with a cryostat. For wild-type and mutant PMC, the concentration of compound I was estimated by the difference in absorbance at 660 nm between compound I and the resting enzyme using a $\Delta\epsilon_{660}$ of 4.5 mM^{-1} cm^{-1}, determined for wt PMC using an excess (∼8 equiv) of peracetic acid to obtain a complete transformation into compound I. The compound II concentration was similarly measured as the difference in absorbance at 435 nm (isosbestic point between compound I and the resting enzyme) between compound II and the resting enzyme using a $\Delta\epsilon_{435}$ of 26 mM^{-1} cm^{-1}. For BLC, the coefficients $\Delta\epsilon_{660}$ [5.7 mM^{-1} cm^{-1} (determined in this study)] and $\Delta\epsilon_{435}$ [32 mM^{-1} cm^{-1} (*28*)] were used to estimate the compound I and II concentrations, respectively. Solutions of peracetic acid were always freshly prepared in 0.2 M acetic acid to limit decomposition.

The rates of NADPH or βNMNH oxidation with catalase submitted to a slow steady flow of H_2O_2 were measured by the decrease in absorbance at 340 nm using an ϵ_{340} of 6.22 mM^{-1} cm^{-1} or an ϵ_{340} of 5.72 mM^{-1} cm^{-1} (*29*) as the extinction coefficient. NADPH assays contained catalase solutions (∼2 μM heme) in 50 mM Tris-HCl buffer (pH 7.5), 2.5 mM $MgCl_2$, 4 mM glucose, and 18 μM NADPH. The reaction was started by adding 2 nM glucose oxidase at 37

°C, giving a steady flow of H_2O_2 of 2 μM/min as measured by the method of Green and Hill (*30*). The same conditions were used with βNMNH except for changing the βNMNH and glucose oxidase concentrations to 232 μM and 8 nM, respectively. Rates of nucleotide oxidation were obtained by averaging three separate measurements. Control rates, determined in the absence of catalase to measure the residual NADPH oxidation rate with the glucose−glucose oxidase system, were subtracted from the values obtained in these experiments.

The NADPH oxidation rate was also determined by the lag duration before the generation of compound II as a function of increasing amounts of NADPH added at the beginning of the reaction, according to the method of Nicholls et al. (*15*). Compound II was generated by the glucose−glucose oxidase reaction with a steady flow of H_2O_2 (2 μM/min) as described for the above assay. The kinetics were recorded at 435 nm to visualize compound II formation.

Simultaneous determinations of compound I decomposition and NADPH oxidation were followed by multiwavelength kinetics in a Cary 50 Bio spectrophotometer. The formation of compound I was performed by addition of 2 equiv of peracetic acid to wt PMC (7 μM heme) in 0.1 M Tris-HCl buffer at pH 7.5 and 22 °C. Under these conditions, no compound II was detected by its typical absorbance at 435 nm (results not shown). Kinetics were simultaneously recorded at 406 and 340 nm to determine the variations in compound I and NADPH concentrations, respectively. NADPH (89 μM) was added when the compound I concentration was at its maximum (minimum of absorbance at 406 nm). A control experiment was carried out without NADPH. The contribution of compound I to the absorbance at 340 nm was calculated according to the following process. The difference Δ [A_{406}(resting enzyme) − A_{406}(compound I)] for each measurement in the presence of NADPH was divided by a coefficient evaluated in the absence of NADPH as Δ [A_{406}(resting enzyme) − minimum A_{406}]/Δ [maximum A_{340} − A_{340}(resting enzyme)]. Similar experiments were carried out using F215Y PMC (7 μM heme), F194Y PMC (4 μM heme), and BLC (8 μM heme).

Crystallization, Data Collection, Structure Determination, and Refinement of PMC Variants. Single crystals of the F194Y and F215Y PMC variants without NADPH were grown by vapor diffusion as previously described for the native enzyme (*31*). High-resolution data were collected from a single frozen crystal per mutant at the European Synchrotron Radiation Facility on the ID14-EH4 beamline. Crystals were soaked for 30 s in a cryoprotecting solution containing 2.8 M ammonium sulfate, 0.8 M sucrose, and 0.1 M Tris-maleate (pH 6.5) and flash-frozen in liquid nitrogen. The structures of mutant enzymes were determined by molecular replacement with the coordinates of the native enzyme without the bound cofactor (Protein Data Bank entry 2CAE) (*19*) as the search model. Integration of data, scaling, and processing were performed with the HKL suite (*32*), and the model was refined with CNS (*33*). The coordinates and the structure factors for both mutant catalases have been deposited in the Protein Data Bank as entries 1H6N and 1H7K for F194Y PMC and F215Y PMC, respectively.

EPR Spectra. CW EPR spectra were recorded with an X-band EMX Bruker spectrometer equipped with an Oxford Instruments ESR 900 helium flow cryostat (*17*). T_1 measurements were performed with a homemade pulsed spectrometer operating at 9.5 GHz. Short pulses (π/2 of 35 ns) were produced with a high-power arm via a 20 W TWT X-band amplificator. For very long pulse durations (up to 0.1 s), a low-power arm, working at 20 mW, was used to eliminate TWT noise. The loop-gap resonator was adapted on an Oxford Instruments helium flow 935 cryostat (temperature range of 1.8−100 K). Temperatures were independently measured by a thermocouple and were given with a precision of better than 0.1 K. The sat−τ−π/2−t−π−echo pulse sequence was used for T_1 determination. The echo intensity was plotted against the delay τ.

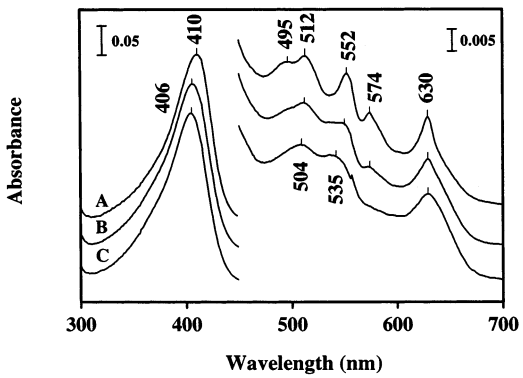

FIGURE 1: Visible spectra of the F194Y and F215Y variants of PMC. Visible spectra at room temperature in 0.1 M Tris-HCl buffer (pH 7.3) of F194Y PMC (A), F215Y PMC (B), and wt PMC (C) for comparison. On the right is the absorbance scale for the Soret band, and on the left is that for the other bands at longer wavelengths. The spectra of F194Y PMC and wt PMC were normalized to that of F215Y PMC.

RESULTS

Spectral Properties and Specific Activities of F194Y and F215Y PMC Mutants. When the optical spectra of the F194Y variant and wt PMC were compared, a slight displacement of the Soret band toward higher wavelengths (410 nm) was observed for the mutant. The peak at 504 nm was replaced by two peaks at 495 and 512 nm (Figure 1). Marked peaks at 552 and 574 nm were also observed, and the peak at 630 nm was narrower than with wt PMC. Similar but less marked changes were also detectable in the F215Y variant. These modifications, also observed in the recombinant PMC, were clearly identified by mass spectroscopy as being caused by the presence of protoporphyrin IX (P. Andreoletti, unpublished data). The F194Y variant had a lower heme content (59%) than the F215Y variant (66%) and other catalases such as wt nonrecombinant PMC and BLC where the heme content (80 and 79%, respectively) was in agreement with previously published results (*34*−*36*) (Table 1).

Due to differences in the heme ratio between the enzymes, the specific activities of the PMC variants with H_2O_2 were reported relative to the heme content (Table 1). The specific activity of F215Y PMC was similar to that of wt PMC, whereas the activity of F194Y PMC was slightly reduced and close to that of BLC.

Crystal Structures of the F194Y and F215Y Variants of PMC. The two mutants crystallized in the same space group ($P6_122$) as native enzymes with similar unit cell dimensions (Table 2). The R_{sym} factors of 10.9 and 8.0 for F194Y PMC and F215Y PMC, respectively, were relatively high. This

Table 1: Specific Catalytic Activity and Heme Content of the Two PMC Variants

catalase	specific activity[a] (mmol of H_2O_2 min^{-1} nmol of $heme^{-1}$)	heme[b] (%)
wt PMC	6.14 ± 0.22	80
F215Y PMC	5.59 ± 0.47	66
F194Y PMC	4.09 ± 0.11	59
BLC	3.89 ± 0.15	79

[a] The specific activities were determined in three independent measurements and quantified on the basis of heme. [b] Percentage of heme in purified tetrameric catalase molecules. The heme content was determined by the pyridine hemochromogen method as described in Experimental Procedures.

Table 2: Crystal Parameters, Data Collection, and Refinement Statistics of F194Y and F215Y PMC Variants[a]

	F194Y PMC	F215Y PMC
space group	$P6_{222}$	$P6_{222}$
cell dimensions (Å)	109.9, 249.78	110.0, 251.2
no. of protein residues/no. of protein atoms	475/3862	475/3862
no. of unique reflections	51135	35932
completeness (%)	98.0 (94.3)	99.7 (99.9)
redundancy	3.9 (2.9)	15.8 (4.8)
R_{sym} (%)[b]	10.9 (37.3)	8.0 (25.1)
refinement		
resolution range (Å)	15−2.1	15−2.4
no. of reflections in the working data set	48584	34138
no. of reflections in the test data set	2551	1794
no. of sulfate ions	1	1
no. of ordered waters	325	180
R_{cryst} (%)[c]	21.5	23.7
R_{free} (%)[d]	24.1	24.0
rms deviation for bonds (Å)	0.008	0.008
rms deviation for angles (deg)	1.4	1.5
cross-validated estimate coordinate error (from Luzzati plot, Å)	0.32	0.34
B-factors at all atoms (Å^2)	53.4	39.7
B-factors at protein atoms (Å^2)	50.3	40.0
B-factors at water atoms (Å^2)	53.1	62.9

[a] Numbers in parentheses refer to the highest-resolution shell. [b] $R_{sym} = \sum_{hkl}\sum_i|I_{hkl,i} - \langle I_{hkl}\rangle|/\sum_{hkl}\sum_i I_{hkl,i}$. [c] $R_{cryst} = \sum_{hkl}||F_{obs}| - |F_{calc}||/\sum_{hkl}|F_{obs}|$, where F_{obs} stands for the observed structure factor amplitudes and F_{calc} for the calculated structure factor amplitudes. [d] A random 5% subset of the data was used for the R_{free} calculation.

can be explained by radiation damage in the crystals due to the high brilliance of the beamline (ID 14-EH4) at ESRF during data collection. This is in agreement with the high R_{sym} factors found at the highest-resolution shell (37.3 and 25.1% for F194Y and F215Y PMC, respectively). The crystallographic structures of the F194Y and F215Y PMC variants were determined at 2.1 and 2.4 Å resolution, respectively. When the structure was compared to the structure of the recombinant enzyme (PDB entry 1E93), rms deviations on the position of all atoms and of the mutated amino acids were 0.29 and 0.28 Å for F194Y PMC and 0.44 and 0.48 Å for F215Y PMC, respectively. The distribution of rather high *B*-factors and pretty high crystallographic *R*-factors (Table 2) can also be explained by radiation damage. However, the mutated residues, Y194 and Y215, exhibited *B*-factors of 44.9 and 43.2 Å^2, respectively, and these values were in agreement with the *B*-factors at protein atoms for Y215 and even lower than the average for Y194 (Table 2). The superimposition of structures of mutated

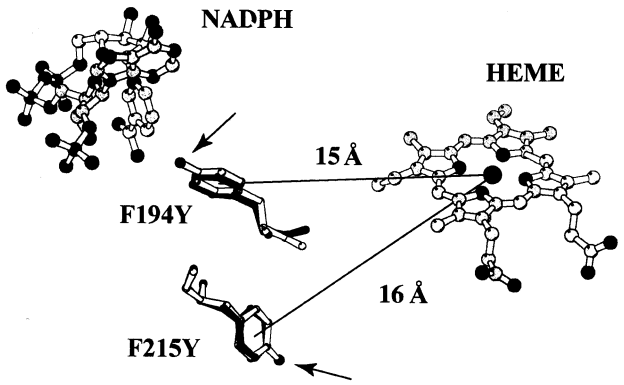

FIGURE 2: Comparison of the structures of phenylalanines 194 and 215 in wt PMC with the corresponding mutated tyrosine residues. The structure of wt PMC with NADPH (PDB entry 2CAH) was used to represent phenylalanines (in black), heme, and NADPH. The structure of tyrosines came from F194Y PMC and F215Y PMC structures determined in this study (PDB entries 1H6N and 1H7K, respectively). The hydroxyl groups of tyrosines with oxygens in black are indicated by arrows. The distances between the heme iron and the geometric center of every tyrosyl phenolic group are given.

tyrosine residues with original phenylalanines from the recombinant enzyme is presented in Figure 2. In both enzymes, the replacement of phenyalanine with tyrosine did not modify either their immediate environment or the global structure of the protein. However, the hydroxyl group of tyrosine 194 in the structure of F194Y PMC was found H-bound to a water molecule (W239 with a *B*-factor of 48.3 Å^2, lower than the average *B*-factor) absent in the structure of both the native recombinant and F215Y PMC enzymes.

Reaction of F194Y and F215Y Variants with Peracetic Acid. The reaction of the two catalase variants (F194Y and F215Y) with peracetic acid was studied by UV−visible spectrophotometry and by EPR spectroscopy. A difference in UV−visible spectra of the PMC variants was observed after reaction for ∼4 min with equivalent amounts of peracetic acid. The spectrum of F215Y PMC exhibited a band at 660 nm characteristic of the green compound I, while that of F194Y PMC had bands at 433, 532, and 567 nm, corresponding to the red compound II. To compare the behavior of the PMC variants with that of unmodified catalases (wt PMC and BLC), the kinetics of formation of compounds I and II were monitored at 660 and 435 nm, respectively (Figure 3). A compound I stable for ∼10 min without formation of compound II was obtained for wt PMC and F215Y PMC (panels A and B of Figure 3, respectively). Under these conditions, BLC also exclusively formed compound I; however, this was spontaneously reduced to the resting state with a half-life of approximately 3 min (Figure 3C). The reaction of BLC with equivalent amounts of peracetic acid at neutral pH (presented in Figure 3) did not lead to the formation of compound II and a tyrosyl radical, as previously observed using high peracetic acid concentrations at acidic pH (*17*). With F194Y PMC (Figure 3D), the simultaneous formation of compounds I and II was observed, and the percentage of compound I reached a maximum, lower than for other catalases, and then decreased continuously with time. In contrast, the level of compound II increased during the first 3−4 min and then slowly decreased, indicating that the enzyme came back to the resting state by spontaneous reduction.

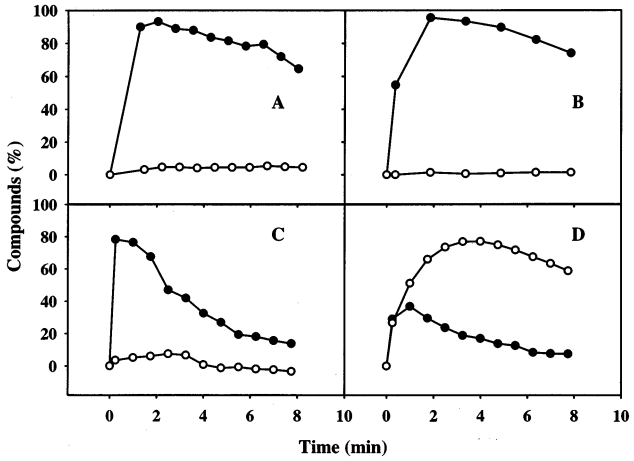

FIGURE 3: Formation and stability of compounds I and II from the PMC variants compared to wt PMC and BLC. Catalase compounds were generated at 22 °C by addition of peracetic acid (1.5 equiv) to enzyme solutions in 0.1 M Tris-HCl buffer (pH 7.5) at the following heme concentrations: (A) 2.1 μM wt PMC, (B) 3 μM F215Y PMC, (C) 2.8 μM BLC, and (D) 1.7 μM F194Y PMC. Spectra were recorded at regular time intervals, and the concentrations of compounds I (●) and II (○) were determined from spectra at 660 and 435 nm, respectively, as described in Experimental Procedures. The percentages of different compounds were calculated considering as 100% the heme concentrations of the starting enzymes.

The reaction of equivalent amounts of peracetic acid with the different catalases was further analyzed by EPR spectroscopy. The EPR spectrum of F215Y PMC, recorded at 4 K, revealed the presence of a signal around $g = 2$, associated with the porphyrin π-cation radical (results not shown). This signal was very similar in both shape and relaxation properties to that recorded with the native enzyme under the same conditions. The disappearance of signal in the $g = 6$ region (the signature of the resting Fe^{3+} state) indicated a total transformation into compound I. The EPR spectrum of F194Y PMC recorded after reaction for >1 min showed no signal that could be attributed either to the iron porphyrin π-cation radical or to the enzyme's resting state. However, another signal in the $g = 2$ region, with relaxation properties characteristic of a radical species, was observed (Figure 4). The hyperfine structure of this signal was nearly identical to that already observed with BLC in the presence of an excess of peracetic acid (*37*). On this basis, the EPR signal obtained with F194Y PMC was assigned to a tyrosyl radical. A quantitative evaluation of the radical concentration gave a maximum value of ~10% of the heme content. A comparison of the saturation behavior at 15 K between the F194Y PMC radical and the tyrosyl radical of BLC indicated that the latter relaxed faster than the F194Y PMC radical. The relaxation properties were further examined by T_1 relaxation measurements at different temperatures. The curves of the echo intensity recorded at 4.2 K with the tyrosyl radicals of BLC and F194Y PMC are represented in Figure 5. The relaxation behavior of a radical interacting with a more rapidly relaxing species in frozen solution did not usually follow a monoexponential decay (*38*). Nevertheless, in the case presented here, the general formula $A[1 - \exp(\tau/T_1)]$ fitted the experimental data quite satisfactorily. From the data (Figure 5), two relaxation times of 0.13 and 0.5 s were obtained for the

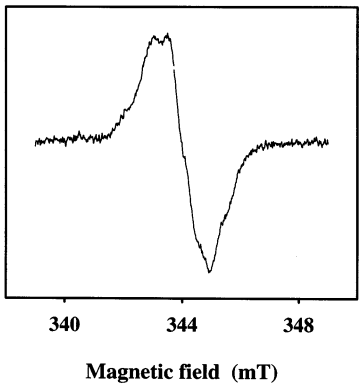

FIGURE 4: EPR spectrum of the tyrosyl radical in F194Y PMC. The tyrosyl radical was generated in an F194Y PMC solution [40 μM heme in 0.1 M Tris-maleate buffer (pH 7.0) and 5% glycerol] after treatment for 1 min with 1 equiv of peracetic acid at room temperature before freezing in liquid nitrogen. Experimental conditions for the EPR spectrum: T of 10 K, microwave power of 10 μW, modulation frequency of 100 kHz, modulation amplitude of 0.3 T, and microwave frequency of 9657 MHz.

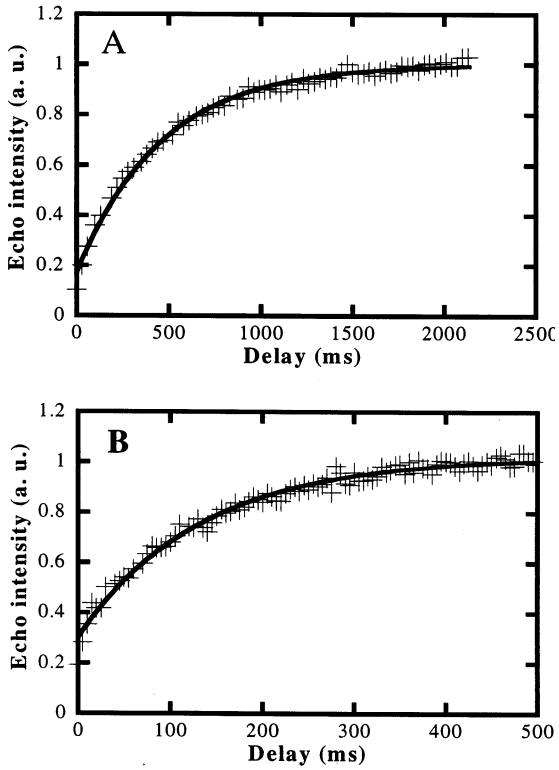

FIGURE 5: Measurements of T_1 for the tyrosyl radicals of BLC and F194Y PMC. The tyrosyl radical was generated in the catalase solutions [~1 mM heme in 0.1 M Tris-citrate buffer (pH 6.2) and 5% glycerol] after treatment for 1 min with 5 equiv of peracetic acid at room temperature before freezing in liquid nitrogen. T_1 measurements by the saturation recovery method for F194Y PMC (A) and BLC (B) at 4.2 K. On the *X*-axis is the delay between the saturation pulse and the $\pi/2-2\pi$ detection sequence (τ). On the *Y*-axis is the intensity of the Hann echo.

tyrosyl radicals of BLC and F194Y PMC, respectively. These times were shorter than that obtained for an isolated tyrosyl radical (*39*).

Reaction of NADPH with Peracetic Acid-Formed Compound I. Wild-type PMC was allowed to react with equivalent amounts of peracetic acid, the effect of NADPH on the transient formation of compound I was followed simulta-

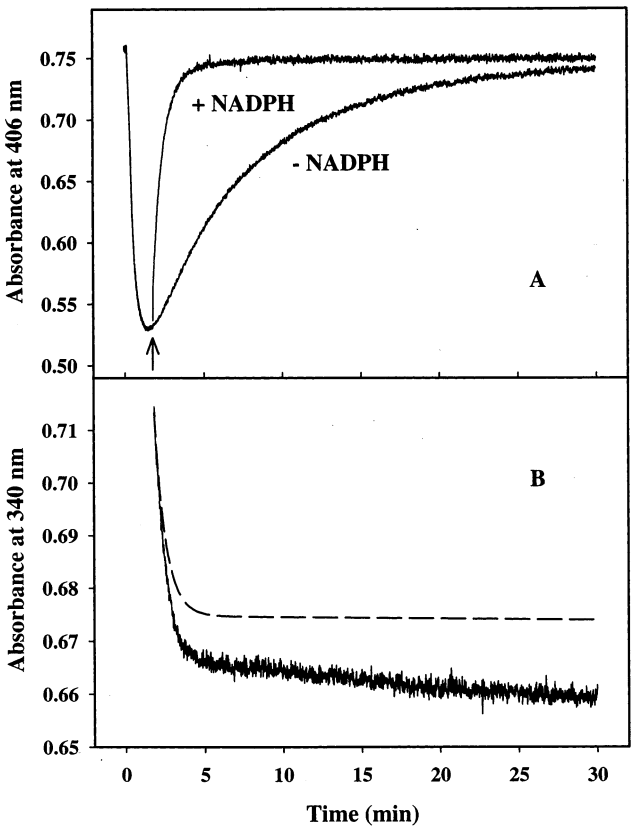

FIGURE 6: Effect of NADPH on the reaction of wt PMC with peracetic acid. The reaction was started by the addition of 2 equiv of peracetic acid to wt PMC (7 μM heme) in 0.1 M Tris-HCl buffer at pH 7.5 and 22 °C. (A) The absorbance was recorded at 406 nm with NADPH (89 μM), which was added when the absorbance was at its minimum (at the arrow) or without NADPH. (B) In the presence of NADPH, the absorbance was simultaneously recorded at 340 nm to follow the oxidation of NADPH. The contribution of compound I to the absorbance (− − −) was calculated as described in Experimental Procedures.

neously at 406 and 340 nm (Figure 6). In the absence of NADPH, the reaction at 406 nm showed a biphasic process, indicating the formation and subsequent spontaneous reduction of compound I (Figure 6A). The curve of compound I reduction fitted a first-order kinetic trace ($k_{obs} = 0.15$ min^{-1}), indicating that the reaction depends only on the compound I concentration. The addition of an approximately 10-fold excess of NADPH when the compound I concentration was maximal (see the arrow in Figure 6A) produced a strong increase in the reduction rate of compound I. The curve of compound I reduction fitted a double-exponential expression to give two rate constants. The rate constant representing the spontaneous reduction of compound I was maintained at a value of 0.15 min^{-1}, as evaluated above. The other calculated rate constant ($k_{obs} = 1.45$ min^{-1}) was ∼10-fold higher than that found without the cofactor. The decrease in absorbance observed at 340 nm indicated that NADPH was oxidized (Figure 6B). The resulting species was $NADP^+$ because it could be recycled into NADPH by an enzymatic system such as glucose-6-phosphate dehydrogenase with glucose 6-phosphate (result not shown). However, to quantitatively estimate the rate of oxidation of NADPH, the contribution of compound I to the absorbance at 340 nm (Figure 6B, dashed line) was evaluated (see Experimental Procedures) and subtracted. The oxidation curve of NADPH could then be fitted to a double-exponential expression from which two rate constants were extracted: $k_{obs1} = 1.67$ min^{-1} and $k_{obs2} = 0.004$ min^{-1}. The highest constant ($k_{obs1} = 1.67$ min^{-1}) represented the NADPH oxidation rate, while the lowest one (k_{obs2}) could be attributed to the spontaneous autoxidation of the cofactor as observed in control kinetics experiments without the enzyme. The rate of NADPH oxidation (1.67 min^{-1}), taking into account the uncertainties of the measurements, was similar to the rate of reduction of compound I measured above (1.45 min^{-1}), showing that the two processes were correlated. Similar results were also obtained with the F215Y variant.

With F194Y PMC, the kinetics were complicated by the simultaneous formation of compounds I and II. The increase in absorbance at 406 nm without NADPH represents mainly the reduction of compound II and not that of compound I. However, in the presence of NADPH, no compound II was formed as shown below. Thus, if NADPH was added before the peracetic acid in the assay, the increase in absorbance at 406 nm corresponded exclusively to the reduction of compound I. The rate constants measured under these conditions at 406 nm ($k_{obs} = 0.87$ min^{-1}) and at 340 nm ($k_{obs} = 0.88$ min^{-1}) were slightly smaller than those obtained with wt PMC.

In a similar experiment conducted with BLC, the following results were obtained. The rate constant of compound I spontaneous reduction ($k_{obs} = 1.38$ min^{-1}) was ∼10-fold higher than the equivalent rate constant found with wt PMC and was increased to a value of 1.80 min^{-1} in the presence of NADPH. The estimated rate constant for NADPH oxidation ($k_{obs} = 1.70$ min^{-1}, corrected for the contribution of compound I) matched well with that of compound I reduction in the presence of the cofactor.

Reactivity of Bovine Liver and P. mirabilis Catalases with Nucleotides. The reaction of wt PMC, the PMC variants, and BLC with NADPH was further analyzed using a steady flow of H_2O_2 produced by the glucose−glucose oxidase system. With wt PMC and the PMC variants, the kinetics of NADPH oxidation, followed at 340 nm, displayed a linear curve (zero-order), and after ∼13 min, an abrupt slowing occurred (Figure 7A). At this point, all the available NADPH was reduced. Increasing the NADPH concentration lengthened the straight line portion without changing the slope (results not shown). These linear kinetics were due to some limiting factor other than NADPH, possibly the compound I concentration. The rate of NADPH oxidation deduced from the slope indicated a minimum value of 0.57 ± 0.02 oxidized NADPH molecule min^{-1} heme^{-1}. The rate found with BLC (0.047 ± 0.005 oxidized NADPH molecule min^{-1} heme^{-1}) was lower than that estimated with PMC, but the kinetics were also linear, indicating that the instantaneous compound I concentration, probably lower than for PMC, remained a limiting factor.

Since rapid compound II formation was characteristic of the F194Y variant, the NADPH oxidation rate of this mutant was also measured by determining the lag preceding compound II formation in the presence of a glucose−glucose oxidase system. As depicted in Figure 8, no compound II was detected in F194Y PMC in the presence of H_2O_2 as long as NADPH was present. The plot of the different lag times against the NADPH concentrations (inset of Figure 8) was linear with a slope of 0.58 oxidized NADPH molecule min^{-1}

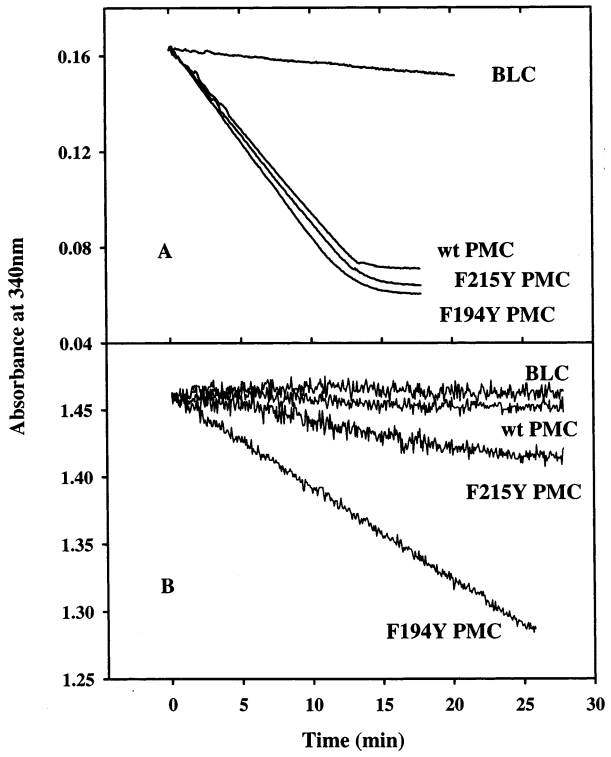

FIGURE 7: Kinetics of nucleotide oxidation by catalases submitted to a slow steady flow of H_2O_2. Catalases (2 μM heme) in aerobic 50 mM Tris-HCl buffer (pH 7.5) and 2.5 mM $MgCl_2$ containing 4 mM glucose at 37 °C. (A) NADPH (30 μM) was added before starting the reaction with a subsequent addition of 2 nM glucose oxidase. (B) Addition of βNMNH (230 μM) before the subsequent addition of 8 nM glucose oxidase. The kinetics were corrected for the spontaneous oxidation of nucleotides.

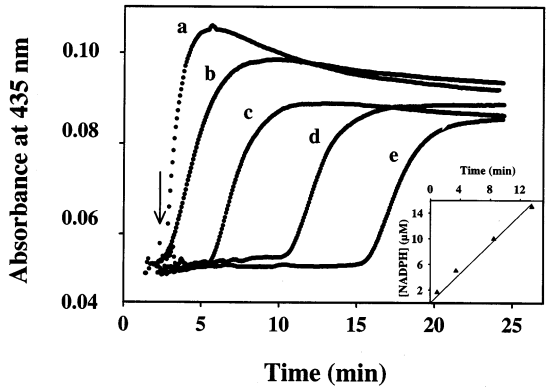

FIGURE 8: Lags in the formation of F194Y PMC compound II caused by the addition of NADPH. The formation of compound II was followed at 435 nm. The reaction mixture (300 μL) contained F194Y PMC (2 μM heme), 50 mM Tris-HCl buffer (pH 7.5), 2.5 mM $MgCl_2$, and 4 mM glucose, and the reaction was started by the addition of 2 nM glucose oxidase (arrow) at 37 °C, generating H_2O_2 at a rate of 2 μM min^{-1}. NADPH was added to the reaction mixture before the glucose oxidase: (a) 0, (b) 2, (c) 6, (d) 12, and (e) 18 μM NADPH, respectively. The lag time was proportional to the amount of NADPH added (inset) and corresponded to the level of NADPH consumption. The calculated rate for NADPH oxidation was 1.16 μM min^{-1} (0.58 oxidized NADPH molecule min^{-1} $heme^{-1}$).

$heme^{-1}$. This clearly confirmed that the same limiting factor as the one evidenced above (Figure 7A) was at work.

All attempts to obtain a higher steady-state compound I concentration relative to catalase by either increasing the H_2O_2 production (increasing the glucose oxidase concentration) or decreasing the catalase concentration were not sufficient to avoid the limitation of the reaction by low compound I concentrations. Other nucleotides having a lower affinity for catalase were used to slow the nucleotide oxidation step. With NADH, known to have a lower affinity for the catalases than NADPH (*20*, *40*, *41*), reactions were very similar to that observed with NADPH. Finally, βNMNH, representing half a molecule of NADPH while retaining the ability to be bound at the same site (result not shown), was assayed in the oxidation reaction. The results indicate that βNMNH did not react with BLC, hardly reacted with wt PMC, and was slightly more efficient with F215Y PMC (Figure 7B). However, a strong increase in the level of βNMNH oxidation was detected with F194Y PMC, and once again, the kinetics were strictly linear and probably limited by the compound I concentration. The reduction rate deduced from the slope was almost the same as with NADPH (0.55 oxidized βNMNH molecule min^{-1} $heme^{-1}$), as expected with a slow steady flow of H_2O_2. This rate, which was a minimum value, was at least 1 order of magnitude faster than the reduction rate measured for the wild-type enzyme with βNMNH (0.058 oxidized βNMNH molecule min^{-1} $heme^{-1}$). However, control lag experiments carried out with F194Y PMC indicated that the presence of βNMNH did not prevent the formation of compound II (not shown). Compound II was also formed by wt PMC, F215Y PMC, and BLC under these conditions.

DISCUSSION

Characterization of PMC Mutants. Two PMC variants (F194Y and F215Y) were successfully overexpressed in *E. coli* and exhibited the same general characteristics as the original wt PMC. However, modifications of UV−visible spectra (Figure 1) showed that protoporphyrin IX was incorporated into the protein structure during folding. The presence of protoporphyrin IX could be explained by an excessive overexpression of catalase in bacteria inducing a deficiency of the endogenous heme. Since the mutant proteins were highly purified, with an Rz index of >1.0, the low heme content found by the pyridine hemochromogen method in the PMC variants was mainly assigned to the presence of protoporphyrin IX replacing the heme group in the protein. However, the possibility of a small proportion of in situ heme degradation as observed in the wild type (*19*, *26*) could not be excluded.

The crystallographic structures of the two PMC variants confirmed the incorporation of tyrosine in place of phenylalanine and the proper folding of both mutant catalases. The replacements only marginally modified the local structure, as evidenced by the same orientation of each aromatic ring (Figure 2).

The specific activities with H_2O_2 of the two PMC variants were roughly the same as that of wt PMC, with the lowest value for F194Y PMC. However, reaction with peracetic acid clearly showed (Figure 3D) that compound I of F194Y PMC was rapidly transformed into inactive compound II, and this could explain the lower specific activity of this mutant.

The concomitant appearance of compounds I and II in F194Y PMC (Figure 3D) indicated that compound I was rapidly reduced to compound II by a single-electron reduction. The simultaneous EPR analysis further supported the

Table 3: Comparison of Dihedral Angles of β Protons and Distances to Heme Iron for Different Tyrosyl Residues in BLC and in F194Y PMC

enzyme[a]	residue	angle 1H (deg)	angle 2H (deg)	distance (Å)
BLC	Y214	−70	55	16
BLC	Y235	−90	26	15
BLC	Y369	−64	58	15
F194Y PMC	Y194	−54	68	15

[a] The angle values and the distances were measured from PDB structure 7CAT for BLC and from this work for F194Y PMC (PDB entry 1H6N). The angles were taken from the normal to the ring plane. The distances were measured between the iron atom and the geometric center of the phenolic group of tyrosines inside a catalase subunit.

conclusion that a tyrosyl residue was the electron donor, resulting in the formation of the radical. The substoichiometric intensity measured by EPR indicated that the tyrosyl radical was submitted to a further reaction restoring a diamagnetic, EPR silent, species. A similar effect of a point mutation was observed with the F172Y mutant of horseradish peroxidase (HRP) where compound I was also destabilized and reduced to compound II by the tyrosyl residue introduced into the protein structure (*42*). The current example demonstrates that the formation of a tyrosyl radical is not solely the result of a short distance between the tyrosyl residue and the heme iron. In HRP, this distance is 10 Å (PDB entry 1ATJ), whereas it is 15 Å in F194Y PMC.

The conclusion that the tyrosyl radical in F194Y PMC was most probably due to the oxidation of Y194 was supported by the following arguments. First, no such radical was observed in wt PMC or F215Y PMC. Second, the dihedral angles formed by the β-protons and the normal to the aromatic ring plane of Y194, as calculated from the X-ray structure (this study), perfectly matched those which were extracted from the measurement of the hyperfine couplings (*17*, *37*). The β dihedral angles corresponding to the tyrosyl radical in F194Y PMC were in perfect agreement with those obtained for the tyrosyl radical in BLC ($\sim$60° in absolute value for each proton) (*37*). Third, the hydroxyl group of Y194 is partially deprotonated by a hydrogen bond with a water molecule, increasing its reducing power (this study).

Localization of the BLC Tyrosyl Radical. Ivancich et al. (*37*) have shown that the tyrosyl radical observed in BLC was relaxed by the iron atom through dipolar and/or exchange interaction(s) between the radical and the iron atom. However, the precise localization of the radical was not definitively solved. The formation of the tyrosyl radical in F194Y PMC allowed us to readdress this problem. Indeed, the relaxation time of the tyrosyl radical in F194Y PMC was $\sim$4 times slower than that of BLC. The comparison of the X-ray structure of this PMC variant with the BLC structure (*43*−*45*) established that, in the two proteins, the relative orientation with respect to the heme and the distance to the iron atom of Y194 in PMC and Y214 in BLC were very similar (Figure 2 and Table 3). The minor structural differences between the two proteins could not produce such important variations in the relaxation times. Furthermore, the heme environment was very similar in both proteins, ensuring the conservation of the relaxation properties of the iron. Consequently, the possibility that the radical in BLC resulted from the oxidation of Y214 must be discarded.

Whatever the precise nature of the interaction between the radical and the iron atom, the distance between both entities in BLC must be of the same order of magnitude or lower than that in F194Y PMC to explain the difference in relaxation times. The analysis of the structure of BLC revealed that only three tyrosine residues could fulfill this condition: Y214, Y235, and Y369 (Table 3). Y369, not conserved in PMC, was the only one with proper orientations of its two β protons with respect to the aromatic ring, i.e., nearly equal dihedral angles (Table 3). This orientation was compatible with the observed equivalence of the two hyperfine couplings (this study). The validity of this argument, previously proposed by Putman et al. (*46*) after examination of the structure of human catalase, is reinforced by the fact that the F215Y mutation of PMC, which is the equivalent of Y235 of BLC, was ineffective in the formation of a tyrosyl radical.

Reaction of Compound I with Nucleotides. The mechanism of reaction of catalases with NADPH is not well understood; in particular, the species (compound I or II) involved in the reaction has not been determined. Until now, it was thought that NADPH could not react rapidly with compound I because compound I was formed in the presence of this cofactor (*13*, *15*). A ratio of compound I to resting enzyme of $\sim$40% was found by Kirkman et al. (*14*) with BLC. The authors also observed that oxidation of NADPH occurred at a rate severalfold greater than the rate of production of compound II which suggests that NADPH can react with compound I itself. Up to now, stable BLC compound I had not been observed during reactions while other oxidation states had appeared (*12*, *14*). In the study presented here, the use of PMC, which is able to form a very stable compound I, led to an improvement in the experimental conditions.

Assays under a slow flow of H_2O_2 clearly pointed toward a limitation of the reaction rate. With NADPH, or even NADH with a lower affinity for catalase, the reaction was so fast that the rate of production of compound I was limiting. Thus, the measured rates (0.57 ± 0.02 and 0.047 ± 0.005 oxidized NADPH molecule min^{-1} $heme^{-1}$ for wt PMC and BLC, respectively) were likely underestimated.

When wt PMC reacted with peracetic acid, measurement of the rate of NADPH oxidation in the presence of a well-defined state of the enzyme was possible. A similarly homogeneous state was also obtained with BLC under the same experimental conditions. NADPH oxidation rates measured with either wt PMC or BLC under these conditions were very similar to the simultaneous reduction rates of compound I. A tight correlation between the two processes was definitively established for the two catalases, strongly supporting the theory that NADPH reacted with compound I.

These results give new insight into the role of NADPH. NADPH had previously been proposed to protect against compound II formation. As another illustration of this effect, the formation of compound II in F194Y PMC under steady-state H_2O_2 production was delayed until complete oxidation of NADPH. The contribution of NADPH to compound II removal was recently estimated to be relatively small (*14*). The protective role of NADPH could now be better explained if NADPH directly reduced compound I into the resting enzyme, thus preventing any partial transformation into inactive compound II. The reaction of NADPH with compound I was faster than the spontaneous decay of compound I into compound II (0.06 min^{-1}) with BLC (*47*). It was

sufficient to fully prevent compound II formation as evidenced with F194Y PMC (this paper) or with BLC (*12*, *15*). The value of the observed rate constant (on the order of 2 min^{-1}) for the reaction of NADPH with compound I was similar for BLC and PMC. This rate is probably well-tuned to ensure the maximum efficiency of compound I reduction, by optimizing NADPH consumption while blocking compound II formation. Following the classification of Nicholls (*48*), NADPH behaves as a two-electron donor like ethanol. Estimation of the second rate constant at the NADPH concentration used in our experiments gave a value of $\sim 3 \times 10^2$ M^{-1} s^{-1}, only slightly inferior to the rate of reaction of ethanol with compound I (10^3 M^{-1} s^{-1} with horse erythrocyte catalase) (*10*).

Since the reduction of compound I by NADPH has now been established, the mechanism of the reaction can be further analyzed by studying the role of catalase tyrosyl radical intermediates.

The observation of a tyrosyl radical must be dissociated from the reaction of NADPH for two main reasons. First, the tyrosyl radical detected in BLC could not be, at least directly, involved in the electron transfer from NADPH to heme because it is localized on Y369, away from the NADPH binding site, and the oxidation of Y369 in BLC was more reminiscent of similar reactions with other hemoproteins such as myoglobin or hemoglobin (*8*, *49*−*51*). Second, the tyrosyl radical detected in F194Y PMC did not facilitate either the oxidation of NADPH or the reduction of compound I of the mutant catalase compared to wt PMC.

In contrast, the presence of a radical on the predicted electron pathway from the nucleotide binding site to the heme (*18*, *22*) was critical for βNMNH oxidation. The nucleotide was rapidly oxidized by F194Y PMC but not by F215Y PMC or wt PMC, neither of which is able to generate a detectable tyrosyl radical. Furthermore, the tyrosyl radical of BLC, located away from the nucleotide binding site, did not favor nucleotide oxidation. Interestingly, F194Y PMC oxidized βNMNH without preventing the formation of compound II. This suggests that the cofactor reduces the tyrosyl radical created in a first step with one electron, thus allowing this tyrosine to be active again in reducing compound I (or possibly compound II). This mechanism may be similar to that described in peroxidases or dioxygenases such as cytochrome *c* peroxidase (*6*, *52*), prostaglandin H synthase (*4*), or linoleate diol synthase (*53*).

In conclusion, two mechanisms can be distinguished in the reaction of nucleotides with catalases: a "direct" mechanism by which the nucleotide reduces compound I in a two-electron reaction and a second "radical-triggered" mechanism, which involves the presence of a radical species and a one-electron process (or two sequential one-electron reactions).

SUPPORTING INFORMATION AVAILABLE

A figure depicting the difference spectra of PMC variants after reaction with approximately stoichiometric amounts of peracetic acid (Figure S1); a figure depicting the positions of three tyrosine residues that are available to carry the tyrosyl radical in the BLC structure (Figure S2). This material is available free of charge via the Internet at http://pubs.acs.org.

REFERENCES

1. Marsh, E. N., and Neil, G. (1995) *BioEssays 17*, 431−441.
2. Stubbe, J., and Riggs-Gelasco, P. (1998) *Trends Biochem. Sci. 23*, 438−443.
3. Lardinois, O. M., and Ortiz de Montellano, P. R. (2000) *Biochem. Biophys. Res. Commun. 270*, 199−202.
4. Koshkin, V., and Dunford, H. B. (1999) *Biochim. Biophys. Acta 1430*, 341−348.
5. Ostdal, H., Andersen, H. J., and Davies, M. J. (1999) *Arch. Biochem. Biophys. 362*, 105−112.
6. Sivaraja, M., Goodin, D. B., Smith, M., and Hoffman, B. M. (1989) *Science 245*, 738−740.
7. McArthur, K. M., and Davies, M. J. (1993) *Biochim. Biophys. Acta 1202*, 173−181.
8. Hanan, T., and Shaklai, N. (1995) *Free Radical Res. 22*, 215−227.
9. Marquez, L. A., and Dunford, H. B. (1995) *J. Biol. Chem. 270*, 30434−30440.
10. Deisseroth, A., and Dounce, A. L. (1970) *Physiol. Rev. 50*, 319−375.
11. Schonbaum, G. R., and Chance, B. (1976) in *The Enzymes* (Boyer, P. D., Ed.) Vol. 13, pp 363−408, Academic Press, New York.
12. Hillar, A., Nicholls, P., Switala, J., and Loewen, P. C. (1994) *Biochem. J. 300*, 531−539.
13. Kirkman, H. N., Galiano, S., and Gaetani, G. F. (1987) *J. Biol. Chem. 262*, 660−666.
14. Kirkman, H. N., Rolfo, M., Ferraris, A. M., and Gaetani, G. F. (1999) *J. Biol. Chem. 274*, 13908−13914.
15. Hillar, A., and Nicholls, P. (1992) *FEBS Lett. 314*, 179−182.
16. Nicholls, P., Fita, I., and Loewen, P. C. (2001) *Adv. Inorg. Biochem. 51*, 51−106.
17. Ivancich, A., Jouve, H. M., Sartor, B., and Gaillard, J. (1997) *Biochemistry 36*, 9356−9364.
18. Olson, L. P., and Bruice, T. C. (1995) *Biochemistry 34*, 7335−7347.
19. Gouet, P., Jouve, H. M., and Dideberg, O. (1995) *J. Mol. Biol. 249*, 933−954.
20. Jouve, H. M., Beaumont, F., Léger, I., Foray, J., and Pelmont, J. (1989) *Biochem. Cell Biol. 67*, 271−277.
21. Gouet, P., Jouve, H. M., Williams, P. A., Andersson, I., Andreoletti, P., Nussaume, L., and Hajdu, J. (1996) *Nat. Struct. Biol. 3*, 951−956.
22. Bicout, D. J., Field, M. J., Gouet, P., and Jouve, H. M. (1995) *Biochim. Biophys. Acta 1252*, 172−176.
23. Andreoletti, P., Franzetti, B., Nussaume, L., Andrieu, J.-P., Gagnon, J., Luche, S., Rabilloud, T., and Jouve, H. (2001) *Can. J. Microbiol. 47*, 130−138.
24. Buzy, A., Bracchi, V., Sterjiades, R., Chroboczek, J., Thibault, P., Gagnon, J., Jouve, H. M., and Hudry-Clergeon, G. (1995) *J. Protein Chem. 14*, 59−72.
25. Samejima, N., and Yang, J. (1963) *J. Biol. Chem. 238*, 3256−3261.
26. Jouve, H. M., Lasauniere, C., and Pelmont, J. (1983) *Can. J. Biochem. Cell Biol. 61*, 1219−1227.
27. Rieske, J. S., Lipton, S. H., Baum, H., and Silman, H. I. (1967) *J. Biol. Chem. 242*, 4888−4896.
28. Gebicka, L., Metodiewa, D., and Gebicki, J. L. (1989) *Int. J. Radiat. Biol. 55*, 45−50.
29. Niviere, V., Fieschi, F., Decout, J. L., and Fontecave, M. (1999) *J. Biol. Chem. 274*, 18252−18260.
30. Green, M. J., and Hill, H. A. (1984) *Methods Enzymol. 105*, 3−22.
31. Jouve, H. M., Gouet, P., Boudjada, N., Buisson, G., Kahn, R., and Duee, E. (1991) *J. Mol. Biol. 221*, 1075−1077.
32. Otwinowski, Z., and Minor, W. (1997) *Methods Enzymol. 276*, 307−326.
33. Brunger, A. T., Adams, P. D., Clore, G. M., DeLano, W. L., Gros, P., Grosse-Kunstleve, R. W., Jiang, J. S., Kuszewski, J., Nilges, M., Pannu, N. S., Read, R. J., Rice, L. M., Simonson, T., and Warren, G. L. (1998) *Acta Crystallogr. D54*, 905−921.
34. Jouve, H. M., Gaillard, J., and Pelmont, J. (1984) *Can. J. Biochem. Cell Biol. 62*, 935−944.

35. Fita, I., and Rossmann, M. G. (1985) *J. Mol. Biol. 185*, 21−37.
36. Lemberg, R., and Legge, J. W. (1943) *Biochem. J. 37*, 117−127.
37. Ivancich, A., Jouve, H. M., and Gaillard, J. (1996) *J. Am. Chem. Soc. 188*, 12852−12853.
38. Rakowsky, M. H., More, K. M., Eaton, G. R., and Eaton, S. S. (1995) *J. Am. Chem. Soc. 117*, 2049−2057.
39. Beck, W. F., Innes, J. B., Lynch, J. B., and Brudvig, G. W. (1991) *J. Magn. Reson. 91*, 12−29.
40. Kirkman, H. N., and Gaetani, G. F. (1984) *Proc. Natl. Acad. Sci. U.S.A. 81*, 4343−4347.
41. Jouve, H. M., Pelmont, J., and Gaillard, J. (1986) *Arch. Biochem. Biophys. 248*, 71−79.
42. Miller, V. P., Goodin, D. B., Friedman, A. E., Hartmann, C., and Ortiz de Montellano, P. R. (1995) *J. Biol. Chem. 270*, 18413−18419.
43. Murthy, M. R., Reid, T. J., III, Sicignano, A., Tanaka, N., and Rossmann, M. G. (1981) *J. Mol. Biol. 152*, 465−499.
44. Reid, T. J., III, Murthy, M. R., Sicignano, A., Tanaka, N., Musick, W. D., and Rossmann, M. G. (1981) *Proc. Natl. Acad. Sci. U.S.A. 78*, 4767−4771.
45. Fita, I., Murthy, M. R. N., and Rossman, M. G. (1986) *Acta Crystallogr. B42*, 497−515.
46. Putnam, C. D., Arvai, A. S., Bourne, Y., and Tainer, J. A. (2000) *J. Mol. Biol. 296*, 295−309.
47. Ferri, A. (1990) *Biochem. Int. 21*, 623−631.
48. Keilin, D., and Nicholls, P. (1958) *Biochim. Biophys. Acta 29*, 302−307.
49. Gunther, M. R., Tschirret-Guth, R. A., Witkowska, H. E., Fann, Y. C., Barr, D. P., Ortiz De Montellano, P. R., and Mason, R. P. (1998) *Biochem. J. 330*, 1293−1299.
50. Davies, M. J., and Puppo, A. (1993) *Biochim. Biophys. Acta 1202*, 182−188.
51. Moreau, S., Davies, M. J., and Puppo, A. (1995) *Biochim. Biophys. Acta 1251*, 17−22.
52. Bonagura, C. A., Sundaramoorthy, M., Pappa, H. S., Patterson, W. R., and Poulos, T. L. (1996) *Biochemistry 35*, 6107−6115.
53. Su, C., Sahlin, M., and Oliw, E. H. (1998) *J. Biol. Chem. 273*, 20744−20751.

BI010687F